Self-Consistent-Field Study of Compressible Semiflexible Melts Adsorbed on a Solid Substrate and Comparison with Atomistic Simulations

Kostas Ch. Daoulas,[†,‡,⊥] Doros N. Theodorou,[*,†,‡] Vagelis A. Harmandaris,[‡] Nikos Ch. Karayiannis,[‡,§] and Vlasis G. Mavrantzas[‡,§]

School of Chemical Engineering, Department of Materials Science and Engineering, National Technical University of Athens, 9 Heroon Polytechniou Street, Zografou Campus, GR 15780 Athens, Greece; Institute of Chemical Engineering and High-Temperature Chemical Processes, ICE/HT-FORTH, GR 26500 Patras, Greece; and Department of Chemical Engineering, University of Patras, GR 26504 Patras, Greece

Received February 1, 2005; Revised Manuscript Received May 2, 2005

ABSTRACT: The present work addresses the problem of a self-consistent-field (SCF) description of a specified polymer melt/solid substrate interfacial system. Key points of the employed method are the coarse-grained representation and the numerical treatment of the continuous-space SCF theory. Compared to other works on polymer adsorption, the main difference of the current approach is the description of the polymer coil connectivity through the wormlike chain model, which, after incorporating local stiffness, reproduces two characteristic lengths of the studied polymer: the mean-squared end-to-end distance and the contour length. As a test case, polyethylene melts adsorbed on a graphite substrate are considered; recent atomistic simulations of the same systems are used to evaluate the theoretical approach. For comparison and elucidation of some effects of chain stiffness on conformational properties of adsorbed molecules, an alternative (and more common) representation of chain connectivity through the Gaussian model, reproducing the mean-squared end-to-end distance, is also considered. Results refer to local and global chain conformational properties, with an emphasis on the latter. In particular, predictions for the shape of chains are obtained, while the conformations of adsorbed molecules are quantified in terms of tails, loops, and trains. For small chain lengths, both the Gaussian and the wormlike chain models deviate considerably from the simulation data. At intermediate chain lengths, however (such as C_{400}), the predictive power of the wormlike model is very good for several conformational properties. On the contrary, predictions from the Gaussian model, especially for the case of loops, deviate considerably from simulations over a broader range of molecular lengths.

1. Introduction

The theoretical description and understanding of properties of polymer melt/solid interfaces are of crucial importance for a variety of technological applications. For instance, the ability to control the quality of products obtained through extrusion and film-blowing operations is closely related to understanding the mechanism behind the cohesive and adhesive failures taking place at the polymer melt/solid interface at high production rates. Controlling the strength of polymer/solid interfaces is also of crucial importance for the technology of adhesives and polymer coatings and for the design of high-performance polymer−solid composite materials.

When developing a theoretical approach for the description of the equilibrium structure and the mechanical properties of a polymer/solid interface, it should be taken into account that this interfacial system incorporates a variety of length scales, starting from the angstrom scale when addressing phenomena in close vicinity to the solid substrate, passing to the nanometer scale when considering polymer density variations, and extending to the submicrometer scale when addressing global polymer chain conformational properties and fracture phenomena.

In this scope, the most sophisticated theoretical tool would comprise a multiscale scheme, combining ab initio calculations for a detailed description of the phenomena taking place in close proximity to the solid substrate with atomistic and coarse-grained simulation techniques to address the nanometer and submicrometer length scales, respectively. If one is interested mainly in large-length scale properties, however, then a coarse-grained approach can by itself provide significant qualitative and quantitative information. In this case, one of the challenges is to choose the coarse-grained representation in such a way that the essential factors determining the physical behavior of the system are still preserved at this level, while a proper correspondence of the characteristic time, energy, and length scales of the coarse-grained model and the prototype system is established.

One of the most common approaches used for the derivation of equilibrium properties of polymer/solid interfacial systems at a coarse-grained level is the self-consistent-field (SCF) method. This approach is particularly powerful and has been used extensively for the prediction of the equilibrium properties of various interfacial macromolecular systems. Apart from this, there is a tendency to employ SCF results as a starting point for the study of these systems away from equilibrium. For instance, SCF results obtained for microphase-separated block copolymer systems in combination with

* To whom correspondence should be addressed at NTU Athens: Tel (+30) 210 772 3157; Fax (+30) 210 772 3112; e-mail doros@central.ntua.gr.
† National Technical University of Athens.
‡ ICE/HT-FORTH.
§ University of Patras.
⊥ Present address: Department of Physics and Department of Chemical and Biological Engineering, University of Wisconsin, Madison, WI 53706.

10.1021/ma050218b CCC: $30.25
Published on Web 07/12/2005

a density-biased Monte Carlo have been employed to create initial configurations for the study of their loading/unloading behavior with molecular dynamics.[1] The mechanical properties of grafted polymer/free polymer melt interfaces have been successfully addressed through polymer entanglement network models,[2] whose generation relies heavily on SCF results.

Although the SCF approach has been used extensively in the past for understanding the equilibrium behavior of polymer solutions and melts in the presence of solid substrates, usually only abstract model systems have been considered. Although the effect of various molecular parameters and thermodynamic state variables on the properties of the interfacial polymeric system could be addressed qualitatively or semiquantitatively (e.g., at the level of scaling relations), the question of establishing a direct correspondence between the coarse-grained model, serving as a basis for the SCF method, and a specified polymeric system has not been covered extensively. To the best of our knowledge, for homopolymer melt/solid interfaces only few lattice-based SCF investigations have been devoted to this question,[3] while hardly any consideration has been given to it with continuous-space SCF.

The essence of the SCF method[4] is in the replacement of the ensemble of the interacting polymer chains with a system of noninteracting polymer molecules subject to some position-dependent chemical potential fields. These fields determine the conformations of the polymer molecules, thereby dictating the spatial distribution of the polymer. On the other hand, the chemical potential fields depend on the polymer distribution. Thus, the whole approach boils down to determining the fields in such a way that they are consistent with the spatial distribution of polymer that they create. One of the essential points of the above scheme is the determination of chain conformations in the mean field, a problem which is ultimately linked to the type of coarse-grained model employed for the representation of the chain connectivity. In the majority of mean-field descriptions of interfacial polymeric systems, the chain connectivity is introduced through the Gaussian model. This considers the polymer chains as fully flexible and infinitely extensible, continuous threads or "paths" and offers the advantage of facilitating the analytical or numerical evaluation of the chain conformations through the solution of the Edwards equation in the mean field. However, the Gaussian model is incapable of describing conformational properties on the length scale of the persistence length, while it additionally fails in accounting for the distal correlation between segments positioned along the chain backbone arising from the chain self-avoidance.[5] In this direction, considerable improvement can be achieved through the implementation of single-chain mean-field theory approaches[6,7] where the characterization of chain conformations in the mean field can be performed using Monte Carlo techniques after accounting for the chain connectivity in the framework of more realistic molecular models (for example RIS) through a "discretized", bead bond, representation of the polymeric chain architecture.

Despite the advantages offered by the single-chain mean-field methods, it is frequently more beneficial to employ continuous thread chain representations due to the relative simplicity of their numerical treatment and the possibility of addressing long-chain length limits at a rather low computational cost. In the realm of continuous thread chain models, a more realistic counterpart to the Gaussian representation is the wormlike model, which treats the molecules as semiflexible threads of prescribed contour length. The mathematical formalism for the implementation of this model in the framework of SCF, even if more complicated in comparison to the Gaussian one, is still quite straightforward.[8,9] Nevertheless, the wormlike model has not met such a wide application.

Several works have shown that the consideration of chain rigidity can affect the predictions for various properties of interfacial polymeric systems. For instance, in the case of block copolymer melts chain rigidity increases the temperature of the order−disorder transition.[10] In tethered polymer/free polymer melt systems the correct incorporation of chain rigidity improves significantly the predictive power of the mean-field theory regarding the properties of the brush/free melt interface.[11] In a polymer adsorption problem, the properties of the molecules are expected to be determined through a balance between the enthalpic gain obtained when the molecule gets close to the attracting substrate and the conformational loss due to the presence of the boundary. The use of a molecular model with internal rigidity and a constrained total contour length can have a substantial effect on the entropic part of this balance, leading to quantitatively different results when compared to the Gaussian case. In addition, the details of the molecular model can influence the way in which adsorbed chains emanate from the substrate, affecting the large length scale structure of the adsorbed layer (formation of loops and tails). Looking from another perspective, it can be said that, through its representation of internal chain rigidity, the wormlike chain, when compared to the Gaussian one,[12] incorporates an additional length scale on the level of the chain persistence length; this can enhance its predictive capabilities with respect to some properties. For very long chains, the large length-scale properties of both the Gaussian and wormlike models are expected to converge to the "exact" properties, as extracted, for example, by atomistic simulation.

In the above framework, the present work is aimed to address the issue of representing a specified polymer/solid interfacial system with a continuous coarse-grained molecular model and subsequently treating it through a SCF approach. Polymer molecules will be considered as wormlike chains. In parallel, the Gaussian model will also be implemented to facilitate the comparison between these two representations and to elucidate some of the effects of chain stiffness on the conformations of adsorbed molecules. Since, to the best of our knowledge, the wormlike chain representation has never been previously employed in a SCF calculation of polymer melt adsorption, one of our basic objectives is the evaluation of the proposed theoretical approach. To this end, the results of recent atomistic simulations[13,14] will be utilized. Without loss of generality, all results of the current study will refer to linear polyethylene melts adsorbed on a graphite substrate.

The article is organized as follows. The next section contains a brief presentation of the atomistic simulations of the polyethylene melt/graphite interfacial systems, which serve as a reference point for the SCF calculations of the current work. Section 3 presents the general SCF theory for the case of adsorbed melts, while section 4 is dedicated to the evaluation of the param-

eters of the mesoscopic representation for the particular case of polyethylene melts adsorbed on graphite. Some general aspects of the numerical treatment of the SCF formalism are discussed in section 5, while additional technical details are contained in the Appendix. Section 6 presents results from the SCF calculations and their comparison with the atomistic molecular dynamics and Monte Carlo simulation data. Finally, the last section summarizes some basic points of the current work.

2. A Brief Description of the Atomistic Simulations and the Studied Systems

A detailed presentation of the molecular dynamics (MD) and Monte Carlo (MC) atomistic simulations of the PE melt/graphite interface, used as a test system for the SCF calculations presented in this work, is contained in refs 13 and 14. For greater clarity, however, we present a brief summary in the following paragraphs.

The atomistic simulations were conducted by describing the PE chains with a united atom model, which considers each methylene (CH_2) and methyl (CH_3) group along the chain backbone as one interaction site. All intramolecular interactions between sites separated by more than three bonds and all intermolecular interactions were described through a 6−12 Lennard-Jones potential parametrized using the TraPPE model[15] parameters for the CH_2/CH_2 interaction (i.e., no explicit distinction was made between the CH_2 and the CH_3 units; they were described by identical pseudoatoms). Regarding the bonded interactions, C−C bond lengths were kept fixed and equal to 1.54 Å, while the bond angles between successive C−C bonds were allowed to fluctuate around an equilibrium angle, $\theta_0 = 114°$, subject to the van der Ploeg and Berendsen potential.[16] Finally, changes of dihedral angles were governed by the Toxvaerd torsional potential.[17] The atomistic representation of the graphite substrate was achieved by describing its interaction with the PE united atoms through a method developed by Steele,[18] which is capable of incorporating the exact crystallographic structure of the graphite. A basal plane of graphite served as the adsorbing surface in all calculations.

The simulations were carried out in orthorhombic cells with periodic boundary conditions along the x and y directions, while the system along the z direction was considered as finite. The polymer was allowed to adsorb on the lower face of the simulation cell, where the graphite substrate was located, thus creating an adsorbed polymer film with its upper surface being exposed to vacuum. The molecular lengths that were considered ranged from C_{40} up to C_{400}, and it was possible to create adsorbed films with thicknesses from 46 up to 125 Å; that is at least 3 times larger than the corresponding equilibrium PE chain gyration radius in the bulk melt. For a thorough equilibration of these systems and the subsequent derivation of their structural, conformational, thermodynamic, and dynamic properties, a hierarchical approach was used. In particular, the equilibration and the derivation of equilibrium static properties were achieved through a robust MC algorithm based on chain connectivity altering moves.[19−21] Subsequently, the equilibrated system was subjected to MD simulations of duration from 20 up to 100 ns, depending on the molecular length and size (total number of atoms) of the simulated system. In this way, apart from deriving the dynamic properties, it was possible to compare MD predictions regarding the static properties of the PE melt/graphite systems against the corresponding results from MC as a test of the statistical mechanical consistency of both approaches and of their ergodicity. In this scope, the agreement between MC and MD methods was found to be excellent.

All melts composed of PE molecules with lengths less than C_{400} were strictly monodisperse, while in the case of the C_{400} melt a small polydispersity was allowed (in particular, a flat molecular weight distribution was realized with polydispersity index $I = 1.0033$) to speed up the equilibration process with the MC method. All atomistic simulations were conducted at a temperature of $T = 450$ K.

3. SCF Theoretical Description of Adsorbed Polymer Melts

One of the major problems appearing during the description of a complex molecular system on a coarse-grained level is associated with the representation of interactions between its constituent entities. In our case of polymer melt/solid interfacial systems the above problem encompasses the following three subproblems: (a) the description of bonded interactions through a suitable definition of chain connectivity, (b) the incorporation of nonbonded polymer/polymer interactions, and (c) the proper definition of the polymer/solid interaction potential.

As was mentioned in the Introduction, in the current work the basic choice for the representation of chain connectivity will be the wormlike (semiflexible) chain model. However, the commonly used Gaussian model will also be considered, in parallel. Comparisons between predictions from the two coarse-grained representations will help elucidate some aspects of the effects of local rigidity on global polymer chain conformational properties. Using the results of the atomistic simulations as a reference point, it will also be possible to establish the limits of applicability of the Gaussian chain connectivity representation. This is of particular practical importance since, as will be seen in the following sections, Gaussian chains constitute much "easier" objects to deal with, numerically, than wormlike chains.

Following ref 22, where a compressible melt near an enthalpically neutral (i.e., hard) wall was considered, the nonbonded interactions will be represented at the coarse-grained level by constraining the polymer density fluctuations around their mean value, characteristic of a "bulk" polymer, through a simple harmonic potential of the form

$$U_{\text{compress}} = \frac{1}{2\kappa}[\phi(\mathbf{r}) - 1]^2, \quad \phi(\mathbf{r}) = \frac{\rho(\mathbf{r})}{\rho_0} \qquad (1)$$

where $\phi(\mathbf{r})$ stands for the polymer volume fraction at point $\mathbf{r}$. The function $\rho(\mathbf{r})$, employed in the definition of volume fraction, is the monomer number density at $\mathbf{r}$, while ρ_0 is the monomer number density in the bulk. Finally, the parameter κ denotes the isothermal compressibility, defined as $\kappa = -V^{-1}(\partial V/\partial p)|_{n,T}$. Note that U_{compress} has the meaning of a free energy density relative to a perfectly homogeneous state at ρ_0, with units of energy per volume. The potential of eq 1, penalizing density fluctuations, was initially employed by Helfand and co-workers[23−25] in their SCF studies of polymer/polymer interfaces and block copolymer sys-

tems. Despite its rather primitive form, it has been shown capable[22] of capturing the combined effects of hard wall and polymer compressibility on chain conformational properties, such as the segregation of chain end-segments to the melt/wall interface. On the other hand, a potential of this form cannot grasp the details of the local structure of the melt, such as the density oscillations close to the solid substrate arising from monomer packing effects, which are successfully described through various density functional theory (DFT) approaches.[26−33] Taking into account this fact, it should be mentioned that a more precise description of local structure can be gained following the practice employed in several works[31−33] through the incorporation of the DFT excess free energy density functionals into the general SCF formalism.

While presenting the mean-field theory for the coarse-grained polymer melt/solid system, the interaction of a "segment" of a Gaussian or wormlike thread with the solid substrate will be described in terms of an arbitrary functional form $U_S(z)$ (with units of energy per segment), where z is the distance of the thread "segment" from the substrate. For greater clarity, the definition of the exact form of this function will be postponed until our discussion of the mean-field description is completed.

The continuum SCF approach is based on a path-integral representation of the partition function. In the past, this approach has been extensively employed in numerous works; the interested reader is referred to several reviews discussing this subject extensively.[4,34,35] Here, an effort will be made to present the theory as briefly as possible, emphasizing only on some essential points specific to the present work. The partition function in the grand canonical statistical ensemble for the case of monodisperse adsorbed melts takes the form

$$\Xi = \sum_{n=0}^{\infty} \frac{1}{n!} \exp\left[\frac{\mu N n}{k_B T}\right] \tilde{N}^n \int \prod_{a=1}^{n} D\mathbf{r}_a(\bullet) P[\mathbf{r}_a(\bullet)] \exp\left(- \frac{1}{2\kappa k_B T} \int [\hat{\phi}(\mathbf{r}) - 1]^2 \, d\mathbf{r} - \frac{\rho_0}{k_B T} \int U_S(z) \, \hat{\phi}(\mathbf{r}) \, d\mathbf{r} \right) \quad (2)$$

where k_B is the Boltzmann constant and T is the temperature, while μ, N, and n are the monomer chemical potential, the degree of polymerization of the coarse-grained molecule, and the number of chains, respectively. $\tilde{N}$ is a normalizing prefactor, and $D\mathbf{r}_a(\bullet)$ denotes functional integration over all possible conformations—"paths"—of the ath chain, while $\hat{\phi}(\mathbf{r})$ is the volume fraction operator, given by

$$\hat{\phi}(\mathbf{r}) = \frac{N \sum_{a=1}^{n} \int_0^1 \delta(\mathbf{r} - \mathbf{r}_\alpha(s)) \, ds}{\rho_0} \quad (3)$$

where s is a scaled variable measuring how far along the contour length of the chain a considered segment lies; it ranges from 0 (chain start) to 1 (chain end). The functional $P[\mathbf{r}_a(\bullet)]$ accounts for the chain connectivity, and in the case of the Gaussian model it takes the form

$$P[\mathbf{r}_\alpha(\bullet)] = \exp\left[- \frac{3}{2R_e^2} \int_0^1 \left(\frac{d\mathbf{r}}{ds}\right)^2 ds \right] \quad (4a)$$

where R_e^2 is the mean-squared end-to-end distance of the polymer chain in the bulk. It can be seen that, in the case of the Gaussian model, only one characteristic conformational parameter of the atomistic polymer chain enters the coarse grained model: R_e^2. For the wormlike chain model the connectivity functional is defined through[8,9,36,37]

$$P[\mathbf{r}_a(\bullet)] = \prod_s \delta(\mathbf{u}^2 - 1) \exp\left[- \frac{\eta}{2N} \int_0^1 \left(\frac{d\mathbf{u}}{ds}\right)^2 ds \right] \quad (4b)$$

where η is a dimensionless bending modulus, while $\mathbf{u}(s)$ is a dimensionless vector, tangent to the contour of the wormlike chain at "segment" s. $\mathbf{u}(s)$ can be defined after invoking the chain contour length L as $\mathbf{u} = (1/L)(d\mathbf{r}/ds)$. Obviously, the product of the delta functions constrains the modulus of the tangent vector to unity, so that the total contour length is preserved. The determination of the prefactor $\eta/2N$ can be better understood if one considers the works of Saito et al.[8] and Chen.[36] In particular, Saito et al. proved[8] that the mean-squared end-to-end distance, R_e^2, of the wormlike chain fulfills the Kratky−Porod relationship:[38]

$$R_e^2 = \left(\frac{\exp(-2DL) - 1 + 2DL}{2D^2 L^2} \right) L^2, \quad DL = \frac{N}{2\eta} \quad (5)$$

By choosing the $N/2\eta$ parameter so that eq 5 is fulfilled, it is possible through the wormlike chain model to reproduce both the contour length, L, and the mean-squared end-to-end distance, R_e^2, of the atomistic polymer molecule. A better understanding of the quantity $N/2\eta$ can be obtained if the limiting case of eq 5 is considered, when $N/2\eta \gg 1$. Then $R_e^2 \approx L/D \rightarrow N/2\eta = L^2/R_e^2$, and it can be seen that the ratio $N/2\eta$ is indeed a measure of the flexibility: the smaller the mean end-to-end distance with respect to the contour length, the more flexible the chain. Obviously, for a freely jointed chain, $\eta = 0.5$. Another convenient representation of the $N/2\eta$ parameter can be gained if one recalls[39] that the ratio R_e^2/L for a polymer molecule, i.e., its Kuhn length, equals twice its persistence length, l_p. Since also $L = Na$, where a is the bond length of the coarse-grained molecule, one gets[9] $\eta = l_p/a$ so that

$$\frac{N}{2\eta} = \frac{L}{2l_p}, \quad \text{when } \frac{N}{2\eta} \gg 1 \quad (6)$$

Following a standard field theoretical approach,[4,34,35,40,41] it is possible to obtain from eq 2 the grand canonical free energy (grand potential), Ω, within the framework of the mean-field approximation. After recalling the translational invariance of the system along the xy plane, the following relationship will hold:

$$\frac{\Omega L_z}{n_{bulk} k_B T} = - \frac{\tilde{N} L_z Q[W] \exp[\mu N / k_B T]}{n_{bulk}} - \int W(z) \, \phi(z) \, dz + \frac{1}{2\kappa k_B T} \frac{V}{n_{bulk}} \int (\phi(z) - 1)^2 \, dz + \frac{V \rho_0}{k_B T n_{bulk}} \int U_S(z) \, \phi(z) \, dz \quad (7)$$

where V is the volume of the system and L_z is its size in the z direction, while the field functional $Q[W]$ denotes the single-chain, Gaussian or wormlike, partition function in the field $W(z)$. For further convenience

in eq 7, we have introduced the parameter n_{bulk} denoting the total number of chains that would be contained in the volume V in absence of any substrate (i.e., in the case of a "bulk" polymer melt). The effective field $W(z)$ and the volume fraction, $\phi(z)$, are coupled to each other through a set of equations depending on the model adopted for the chain connectivity. For the case of the wormlike chains, after recalling the translational invariance along the xy plane, these equations are formulated as

$$W(z) = \frac{V[\phi(z) - 1]}{\kappa k_B T\, n_{bulk}} + \frac{\rho_0 V U_S(z)}{n_{bulk} k_B T} \tag{8a}$$

$$\phi(z) = \frac{2\pi\tilde{N}V \exp[\mu N/k_B T]}{n_{bulk}} \int_{-1}^{1}\int_{0}^{1} q(z, s, \cos\theta)\, q(z, 1 - s, -\cos\theta)\, ds\, d\cos\theta \tag{8b}$$

where the quantity $q(z, s, \cos\theta)$, when multiplied by the surface of the xy plane, equals the single-chain partition function of the $(0,s)$ portion of the chain under the restrictions that (a) the s segment is found at a distance z from the substrate and (b) the cosine of the angle formed by the z axis and the tangent vector at s is equal to $\cos\theta$. The $q(z, s, \cos\theta)$ propagator can be calculated through an equation, introduced[8] by Saito et al., which is the analogue of the Edwards equation for wormlike chains:

$$\frac{\partial q}{\partial s} + L\cos\theta\,\frac{\partial q}{\partial z} = \frac{N}{2\eta}\frac{1}{\sin\theta}\left[\cos\theta\,\frac{\partial q}{\partial\theta} + \sin\theta\,\frac{\partial^2 q}{\partial\theta^2}\right] - W(z)q \tag{9}$$

with initial condition[9,10,37] $q(z, 0, \cos\theta) = 1$. The boundary condition at $z = L_z$ is conveniently determined after setting the value of the field $W(L_z) = 0$ so that $q(z = L_z, s, \cos\theta) = 1$. After defining the $W(z)$ field as zero at L_z and considering that far from the substrate the polymer volume fraction should be unity, i.e., $\phi(L_z) = 1$, the value of the multiplying prefactor in eq 8b is determined as $2\pi\tilde{N}V \exp[\mu N/k_B T] n_{bulk}^{-1} = 1/2$.

The boundary condition at $z = 0$ requires some further discussion. Commonly,[42−44] when considering questions related to polymer adsorption, the Edwards equation is supplied with an effective boundary condition. This practice originates from the work of de Gennes[45] and amounts to splitting the total effective field felt by a polymer segment into a part originating from its interaction with the substrate and a mean-field part accounting for the interactions with the rest of the polymer segments. (The latter is sometimes denoted[42] as "the molecular field".) Then, the surface potential is disregarded, and its presence is taken implicitly into account when solving the Edwards diffusion equation in the remaining mean-field component, by imposing on the propagator Q an effective boundary condition: $(1/Q)(\partial Q/\partial z)|_{z=0} = -c$. The parameter c is the inverse of the extrapolation length, specifying the segment/surface interactions.[42,44] In our case, however, we will preserve the surface component of the effective field $W(z)$. To this end the propagator equation, eq 9, has to be supplied with a "true" boundary condition and not with an effective one. This boundary condition is the so-called "absorbing boundary condition", requiring $q(z = 0, s, \cos\theta) = 0$. We would like to complete this discussion of boundary conditions by referring the interested reader to the work[22] of Wu et al. considering a polymer melt near an enthalpically neutral substrate, where a detailed presentation is given of how, beyond some distance from the wall, the microscopic absorbing boundary condition effectively reduces to the well-known for this case, reflecting boundary condition.

Equations 8a and 8b in combination with the propagator equation, eq 9, supplemented with the proper initial and boundary conditions, constitute a closed system of SCF equations describing the polymer melt/solid substrate interfacial system at the level of the wormlike molecular model.

In the case of the Gaussian model the essence of the approach remains the same. In particular, eq 8a will remain the same while eq 8b transforms to

$$\phi(z) = \frac{\tilde{N}V \exp[\mu N/k_B T]}{n_{bulk}} \int_0^1 q(z,s)\, q(z, 1 - s)\, ds \tag{10}$$

Finally, instead of eq 9, the propagator will fulfill the Edwards equation

$$\frac{\partial q}{\partial s} = \frac{R_e^{\,2}}{6}\nabla^2 q - W(z)q \tag{11}$$

with the same initial and boundary conditions: $q(z, 0) = 1$, $q(0, s) = 0$, and $q(L_z, s) = 1$.

Having cast the SCF framework, it is now possible to proceed with the exact definition of the parameters entering the theoretical formalism, including the description of polymer/substrate interactions and the numerical approach for solving the SCF set of equations.

4. Representation of the PE Melt/Graphite Interfacial System with the Wormlike Chain Molecular Model

After the set of SCF equations (eqs 8a, 8b, and 9) has been formulated, there are several parameters to be determined so that a correspondence between the coarse-grained and the atomistic PE/graphite systems can be established. Not all of these parameters have to be specified, however, since only some combinations of them will have an actual physical meaning in the framework of the mesoscopic representation.[24,46] These combinations, which are called *invariants* after Helfand and Sapse,[24] will retain values characteristic of the atomistically simulated polymeric system, establishing the equivalence of its characteristic length and energy scales to those of the coarse-grained system.

Since all atomistic simulations were performed at $T = 450$ K, the same temperature will be assumed during the SCF calculations of the current work. The current mesoscopic representation will preserve the volume, V, of the system as well as the number of the chains, n_{bulk}. To this end, both the mesoscopic and the atomistic systems, in the "bulk", have the same number of chains per unit volume: n_{bulk}/V, which can be trivially calculated from the molecular weight and the bulk density, ρ_{bulk}, of the atomistic system. In all calculations of this work $\rho_{bulk} = 0.766$ g/cm^3. The pressure p is also set as invariant, so the compressibility of the mesoscopic system, being defined as $\kappa = -V^{-1}(\partial V/\partial p)|_{n,T}$, will equal the isothermal compressibility of the atomistically studied polymer. Taking into account the atomistic simulation[20] results and experimental data,[47] we employed $\kappa = 1.43 \times 10^{-9}$ Pa^{-1}.

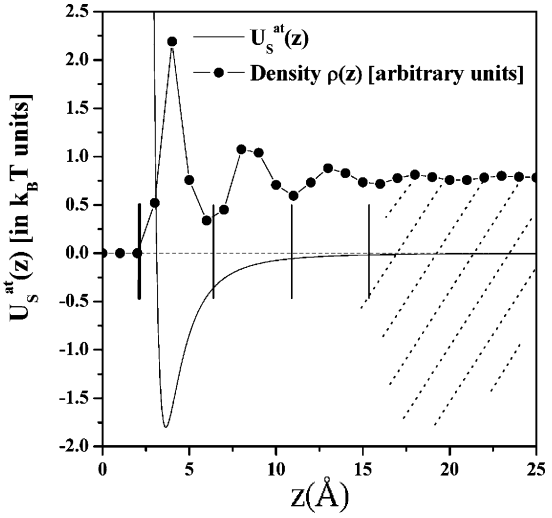

Figure 1. z dependence of the atomistic PE monomer/graphite interaction potential, $U_s^{at}(z)$ (solid line), plotted for a CH_2 unit lying directly above the center of a graphite hexagon and its effect on local polymer density (shown in arbitrary units, by the small solid circles). The large, thickly drawn first vertical bar shows where the first layer of graphite carbon atoms ends, while the average positions of the CH_2 units in the three adsorbed polymer layers are situated between the remaining three vertical bars (shown as thin lines).

Following the previous section, the length scales of the mesoscopic and the atomistic molecular models are related through two invariant parameters: the contour length of the chain, L, and the mean square end-to-end distance of the chain, R_e^2. Both of them can be evaluated as

$$L = n_b l_b \sin(\theta_0/2), \quad R_e^{\,2} = C n_b l_b^{\,2} \tag{12}$$

where n_b, l_b, θ_0, and C denote the number of chemical bonds, the bond length, the equilibrium bond angle along the chain backbone, and the polyethylene characteristic ratio, respectively. In the current work, the values $l_b = 1.54$ Å and $\theta_0 = 114°$ have been used, while C was calculated taking into account its dependence on the number of carbon atoms in the PE molecule, N, as $C = a_0 + [a_1/(N-1)] + [a_2/(N-1)^2] + [a_3/(N-1)^3]$. The coefficients a_0, a_1, a_2, and a_3 are constants, being equal[48] at $T = 450$ K to 8.27, −43.59, −246.02, and 3182.6, respectively.

After the parameters L and R_e^2 are known, the ratio $N/2\eta$ can be evaluated either by solving numerically the Kratky−Porod relationship, eq 5, or by using the limiting eq 6, if the condition $N/2\eta \gg 1$ holds. For all systems studied here, the values of $N/2\eta$ calculated from the Kratky−Porod equation, eq 5, and from its approximation, eq 6, were found to be practically the same, particularly for the larger molecular weights. For instance, for the relatively "short" C_{78} melt, the exact Porod−Kratky equation gives $N/2\eta = 6.24$, while the approximation leads to $N/2\eta = 6.78$.

The last step for the accomplishment of the mesoscopic representation of the PE/graphite system is the definition of the polymer/substrate interaction potential, $U_s(z)$. In this scope, we recall the z dependence of the atomistic PE monomer/graphite interaction potential, $U_s^{at}(z)$, and its effect on the polymer density, both presented in a collective graph in Figure 1 for an adsorbed C_{250} melt. For small z, the $U_s^{at}(z)$ potential is repulsive, accounting for the excluded-volume interactions between the polymer monomers and the atoms of the graphite lattice (in Figure 1 the thickly drawn first vertical bar shows where the first layer of graphite carbon atoms ends), while further in it assumes the form of a localized attractive well. Practically, the range of the well is around 15 Å, resulting in the emergence of three sharply structured layers of adsorbed polymer segments, positioned between the thin vertical bars of Figure 1. Beyond $z = 15$ Å the local density tends to assume a constant value, equal to the density of the bulk melt. To represent the strong polymer/graphite repulsion within the first 2 Å in the SCF calculations, we shift the origin of the z-axis [where $q(z = 0, s, \cos\theta) = 0$] with respect to the atomistic system by 2 Å; thus, the strongly repulsive part of the $U_s^{at}(z)$ is approximated with an impenetrable wall. Taking into account the localized character of the attractive part of the $U_s^{at}(z)$ potential, we represent it on the coarse-grained level through a simple square well, which is completely defined when its width, w, and depth, U_0, are known. The width is determined after observing that, in the atomistic density profile of Figure 1, the most significant adsorption peak is the first one. In addition, an analysis of the atomistic simulation results reveals[13] that a considerable percentage of the atoms found in the next two peaks (70% for the second and 44% for the third) belong to chains passing from the first adsorption layer. Taking into account all this information, the width w is set equal to the width of the first adsorption peak, that is $w = 4.5$ Å.

To determine the depth of the square well potential, U_0, we require the coarse-grained PE/graphite system to have the same adsorption energy, E_{ads}, per unit surface as the atomistic one (i.e., we choose the adsorption energy per unit surface as an invariant of the mesoscopic representation). This requirement is expressed as

$$E_{ads} = -0.25 k_B T/\text{Å}^2 = \rho_0 \int U_S(z)\, \phi(z)\, dz = \frac{n_{bulk} N U_0}{V} \int_0^w \phi(z)\, dz \tag{13}$$

where the value $E_{ads} = -0.25\ k_B T/\text{Å}^2$ was determined from the atomistic simulation. A careful consideration of the SCF equations (eqs 8a, 8b, and 9) and the integral constraint of eq 13 reveals that the polymerization degree, N, of the coarse-grained chain never appears by itself but always in combination with some other quantity; thus, N is not an invariant of the representation. For instance, in eqs 8b and 13 it appears in combination with the U_0 parameter. In this way, one actually has to determine the product NU_0 entering eqs 8b and eq 13 and not the U_0 parameter by itself. Obviously, the determination of NU_0 from eq 13 requires knowledge of the volume fraction profile, $\phi(z)$, as derived from SCF theory. Thus, the NU_0 reproducing the desired adsorption energy has to be determined through an iterative scheme: one starts from some initial guess value, solves the SCF set of equations as described in the following section, determines $\phi(z)$, and evaluates E_{ads}. If the result is not the desired one, the NU_0 is corrected by some small quantity and the procedure is repeated, until the correct adsorption energy is obtained. The value of NU_0 has to be defined only for one molecular weight, C_{78} for example: For the rest systems it is derived by multiplying this "base case" NU_0 value

by the ratio of the molecular weight of the melt under study to the molecular weight of the base case.

5. Solution Method

The SCF equations formulated in the current work (i.e., eqs 8a, 8b, and 9 or, alternatively, eqs 8a, 10, and 11 if the Gaussian model is invoked) can be solved following a simple relaxation technique similar to the one employed in ref 49. An initial guess for the field $W(z)$ is made (usually a random one) which is substituted into the propagator equation (eqs 9 or 11). Subsequently, the equation is solved numerically so that the propagator, q, is found, and the corresponding spatial distribution of polymer, given by the volume fraction $\phi(z)$, is calculated from eq 8b or eq 10 (depending on the model). Then a new value for the field is established as $W^{new}(z) = W(z) + \lambda[W(z) - \tilde{W}(z)]$, where the $\tilde{W}(z)$ is evaluated after substituting the calculated volume fraction $\phi(z)$ into eq 8a. The new field value serves as an input for the next iteration step, and the whole procedure, described previously, is repeated again. The iteration continues until convergence is achieved, being commonly confirmed by monitoring the behavior of the free energy (eq 7); in the current work the iterative scheme was considered converged when the relative free energy change between two sequential iterations was on the order of 10^{-12}. The magnitude of the relaxational parameter λ is determined empirically so that the stability of the calculations is preserved. As a rule of thumb, it is mentioned that its magnitude is inversely related with the value of the $V/\kappa k_B T n_{bulk}$ prefactor in eq 8a: the larger the molecular weight of the studied melt, the smaller the λ that can be employed. For example, for a C_{78} system a value of $\lambda = 0.001$ can be used, while in the case of a C_{1000} melt it has to be reduced to 0.0005 to maintain stability.

The central component in the above iteration scheme is the numerical solution of the propagator equation (eq 9 or eq 11). For the Gaussian molecular model, the one-dimensional Edwards diffusion equation can be solved through a Crank−Nicholson approach,[50,51] for instance. The case of the wormlike chain model presents more difficulties and will be discussed more extensively in the following.

For the wormlike model we proceed with the solution of the propagator equation, eq 9, expanding the propagator function, $q(z = 0, s, \cos\theta)$, in terms of Legendre polynomials after the recommendations of refs 10 and 37:

$$q(z, s, \cos\theta) = \sum_{m=0}^{\infty} \tilde{q}_m(z,s)\, P_m(\cos\theta) \qquad (14)$$

This expansion is substituted into eq 9, which is afterward multiplied by the lth Legendre polynomial[37] ($l = 0, 1, ..., \infty$) and integrated over the variable $\cos\theta$. Taking into account the properties of Legendre polynomials (i.e., orthogonality and recurrence relationships), it is possible to prove that the expansion coefficients satisfy the following set of partial differential equations:

$$\frac{2\eta}{N}\frac{\partial \tilde{q}_l}{\partial s} = -\left[\frac{l}{2l-1}\frac{\partial \tilde{q}_{l-1}}{\partial z} + \frac{l+1}{2l+3}\frac{\partial \tilde{q}_{l+1}}{\partial z}\right] - (l+1)l\tilde{q}_l - \frac{2\eta}{N}W(z)\tilde{q}_l, \quad l = 0, 1, ..., \infty \qquad (15a)$$

with initial and boundary conditions

$$\tilde{q}_l(z = 0, s) = 0, \quad \tilde{q}_l(z = L_z, s) = \delta_{l,0}, \quad \tilde{q}_l(z, s = 0) = \delta_{l,0} \qquad (15b)$$

where the $\delta_{\alpha,\beta}$ is the Kronecker symbol. In eq 15a all lengths are expressed in units of $2\eta L/N$, which, for large molecular lengths, will be twice the persistence length (see eq 6).

The propagator differential equation, eq 9, is now replaced by the set of eqs 15, which has to be solved numerically at each iteration.

To the best of our knowledge, the approach for the solution of this problem, appearing in various applications of semiflexible chains to interfacial polymeric systems, has not been extensively presented in the literature. Moreover, although in a recent work[52] considering melts of semiflexible diblock copolymers a forward time-centered space (FTCS) scheme was successfully employed for a similar numerical problem, exploratory runs showed that in the case of adsorbed polymer melts this approach leads to a strong instability near the solid boundary. In view of this, in this work a Lax−Wendroff-like approach[53] was developed for the numerical treatment of eqs 15. The implementation of this technique requires the truncation of the Legendre polynomial series which, taking into account ref 37, in the current SCF calculations was set at $m = 8$ (that is, $\tilde{q}_8 = 0$). This choice was further justified by test calculations employing a higher expansion order ($m = 13$), which led practically to the same results. As a general comment it can be said that the stability of the suggested method was discovered to be dependent on the relevant magnitude of the descretizations employed for the 1D-coordinate space and the chain contour length: in the case of large chain lengths (corresponding to large absolute mean-field values close to the wall and large values of the parameter $N/2\eta$) a significant increase in the chain contour discretization was required in order to maintain a resolution level along the space coordinate similar to the one used for shorter chain lengths. As an example, we mention that to provide the calculations in the C_{1000} melt with a space resolution on the order of 1 Å, the discretization along the chain contour had to be kept around 6×10^{-4}. A similar level of space resolution in the case of C_{5000} melt could be achieved only when the chain contour discretization was on the order of 1×10^{-4}.

We avoid further presentation of these rather technical issues in the main text, referring the interested reader to the Appendix, where a more detailed discussion can be found.

6. Results

Local Volume Fraction. The local volume fraction, $\phi(z)$, derived from the SCF calculations for the C_{250} PE melt/graphite system is presented in Figure 2, where for comparison the atomistic simulation result is also shown. The two vertical dashed lines delimit the area where the polymer is subjected to the effect of the attractive, square well, part of the coarse-grained polymer/graphite potential, $U_S(z)$. Because of the absence of the microscopic single monomer size length scale from the wormlike and the Gaussian chain models, in combination with the simplified description of the intermolecular interactions, the SCF calculation should not be expected to reproduce phenomena taking place

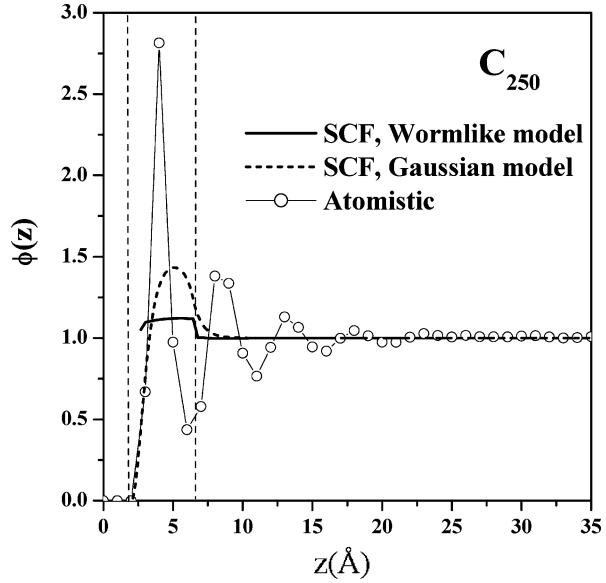

Figure 2. Polymer volume fraction profile, $\phi(z)$, as derived by the SCF theory after the implementation of the wormlike (solid line) and the Gaussian (thick dashed line) chain connectivity models. The vertical, thin dashed lines enclose the region where the polymer is subjected to the effects of the attractive square well potential in the coarse-grained description, while the open circles correspond to the atomistic simulation data.

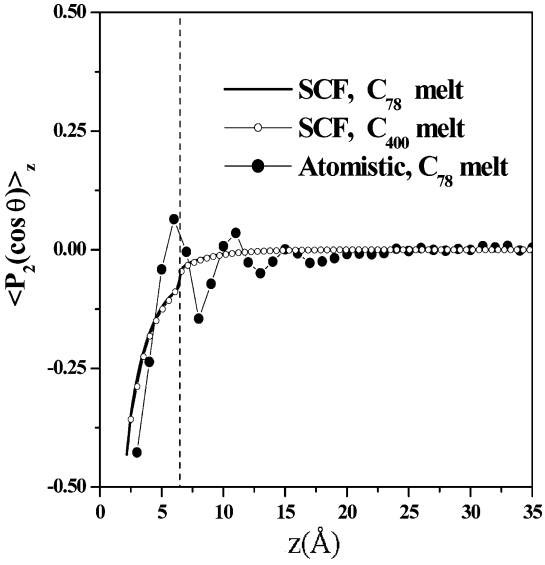

Figure 3. Local bond order parameter, $\langle P_2(\cos\theta)\rangle$, calculated as a function of distance, z, from the adsorbing substrate by application of the wormlike chain SCF approach for two melts: C_{78} (solid line) and C_{400} (open circles). The corresponding prediction of the atomistic simulations for the order parameter of the C−C bonds is denoted by solid circles. The vertical, thin dashed line denotes the boundary of the region where the polymer is subjected to the effects of the attractive square well potential in the coarse-grained description.

on atomistic length scales. The SCF calculations of this work cannot reproduce the oscillatory behavior of $\phi(z)$ close to the substrate, observed during the consideration of the system with atomistic simulations. Qualitatively, however, the SCF approach provides a reasonable smoothed picture of polymer density variations in the area subjected to the effect of the potential $U_S(z)$ in the form of a single adsorption peak, where the polymer volume fraction is $\approx$1.1. A similar result is derived when the atomistic polymer volume fraction profile is averaged on a more "coarse-grained scale": An average over the first adsorption peak yields $\phi = 1.22$. For comparison, on the same figure we reproduce the $\phi(z)$ profile derived with the Gaussian connectivity model, wherein the well depth of the coarse-grained interaction potential $U_S(z)$ was also tuned to reproduce the correct adsorption energy. In this case the adsorption peak is more pronounced, while a strong depletion can be observed close to the boundary, despite the attractive interactions with the substrate. This depletion, which is much more significant in the case of the Gaussian chain melt than in the wormlike chain model, has an entropic origin, i.e., is due to the loss of conformations of the polymer chain close to the substrate. This difference between the two models can be explained after considering the infinite extensibility of segments in the Gaussian chain model. This should allow stronger variations of polymer density on a bond-size length scale, thus favoring a smooth transition from complete absence of polymer near the substrate to a well-formed adsorption peak, a few angstroms away.

Local and Overall Chain Conformational Properties. A typical measure of the effects of the solid substrate on the conformations of the polymer chains, when considered on the level of individual bonds, is the bond-order parameter $P_2(\cos\theta)$. More specifically, P_2 corresponds to the second-order Legendre polynomial, while θ denotes the angle between the bond and the z-axis. This parameter is of particular interest since it can be measured experimentally through deuterium NMR experiments,[54] so a direct connection with the theoretical predictions can be established. In the case of the currently studied adsorbed melts the average of this parameter was evaluated for the wormlike chain model as a function of bond distance from the adsorbing substrate as

$$\langle P_2(\cos\theta)\rangle_z = \int_0^1\int_{-1}^1 w(z, s, \cos\theta)\, P_2(\cos\theta)\, \mathrm{d}\cos\theta\, \mathrm{d}s$$

$$w(z, s, \cos\theta) = \frac{q(z, s, \cos\theta)\, q(z, 1-s, -\cos\theta)}{\int_0^1\int_{-1}^1 q(z, s, \cos\theta)\, q(z, 1-s, -\cos\theta)\, \mathrm{d}\cos\theta\, \mathrm{d}s} \quad (16)$$

where the propagator $q(z, s, \cos\theta)$ is derived from eqs 14 and 15a after substituting the converged solution of the SCF scheme, $W(z)$. The function $w(z, s, \cos\theta)$ denotes the probability density that the cosine of the angle formed by the tangent vector to a "segment" located at position s along the wormlike chain backbone is equal to $\cos\theta$, under the condition that this segment is found at distance z from the substrate. (The numerator of w denotes the total number of "paths" satisfying this condition, while the denominator represents the total number of paths crossing z, irrespective of the position along the chain contour and the tangent vector orientation where this intersection occurs.) The integrals in eq 16 can be conveniently evaluated after substituting the expansion of the propagator over the Legendre polynomials, eq 14, and invoking their orthogonality property as well as their recurrence relationships.

The $\langle P_2(\cos\theta)\rangle_z$ function derived in this way using the wormlike chain model is presented in Figure 3 for two adsorbed melts C_{78} and C_{400}, while, for comparison, the atomistic simulation data for the C_{78} melt are also shown. It can be seen that the bond order parameter is a "local" property, being unaffected by the chain molec-

ular weight. Close to the graphite $\langle P_2(\cos\theta)\rangle_z$ attains large negative values, characteristic of a parallel orientation of the segments of the wormlike chain with respect to the adsorbing substrate. $\langle P_2(\cos\theta)\rangle_z$ increases monotonically over a length scale equal to the width of the attractive well to become zero a few angstroms away from the domain of polymer/substrate attraction, manifesting a loss of any orientation at the bond level at distances that are large compared to the segment size and to the range of the potential. The discontinuity of $\langle P_2(\cos\theta)\rangle_z$ at the border of the attractive well is due to the functional form of the $U_S(z)$ potential. Similar results obtained with alternative, smooth $U_S(z)$ functions reproducing the same adsorption energy with a similar length scale of polymer/substrate attraction did not exhibit such a discontinuity, while the behavior of $\langle P_2(\cos\theta)\rangle_z$ in the rest of the domain remained practically the same. In contrast to the SCF results, the atomistic simulation data exhibit an oscillation between negative and positive values of $P_2(\cos\theta)$; the latter values are somewhat smaller in magnitude. This oscillation is commensurate with the variations of the density near the substrate (see also Figure 1), originating in the specifics of local monomer packing. Despite the intrinsic incapability of the current coarse-grained molecular model to account for these packing effects, it can be observed that the SCF can indeed reproduce the average trend of the atomistically derived curve, leading to very similar values of $\langle P_2(\cos\theta)\rangle_z$ close to the adsorbing boundary.

The effect of the adsorbing substrate on global chain conformational properties can be elucidated after analyzing the shape of the chains in the various parts of the PE melt/graphite interfacial system. A direct measure of this property at any distance, z_0, from the substrate is provided by the number of chains per unit surface passing through a plane placed at z_0 parallel to the attractive surface.[55] In particular, the probability, $p_{\text{cross}}(z_0)$, that a chain starting anywhere in the system will intersect the given plane can be calculated as

$$p_{\text{cross}}(z_0) = 1 - \frac{\int_0^{z_0}\int_{-1}^{1} q_1(z, 1, \cos\theta)\,\mathrm{d}\cos\theta\,\mathrm{d}z + \int_{z_0}^{L_z}\int_{-1}^{1} q_2(z, 1, \cos\theta)\,\mathrm{d}\cos\theta\,\mathrm{d}z}{\int_0^{L_z}\int_{-1}^{1} q(z, 1, \cos\theta)\,\mathrm{d}\cos\theta\,\mathrm{d}z} \tag{17}$$

where the propagators $q_1(z, s, \cos\theta)$ and $q_2(z, s, \cos\theta)$ describe the conformations of the wormlike chain contained below or above the dividing z_0 plane, respectively, without intersecting it. These propagators can be obtained from eq 9 (in practice, from the equivalent form, eq 15a,b) after substituting the converged solution of the SCF scheme, $W(z)$, in the two regions $0 < z < z_0$ and $z_0 < z < L_z$. The initial and boundary conditions for the fist region are $q(z, 0, \cos\theta) = 1$, where $0 < z < z_0$ and $q(0, s, \cos\theta) = 0$, $q(z_0, s, \cos\theta) = 0$, while in the second region $q(z, 0, \cos\theta) = 1$, where $z_0 < z < L_z$ and $q(z_0, s, \cos\theta) = 0$, $q(L_z, s, \cos\theta) = 1$. After the p_{cross} is evaluated, the number of chains, $n(z_0)$, per unit surface that intersect the plane at z_0 is obtained as

$$n(z_0) = p_{\text{cross}}(z_0)\left[\frac{n_{\text{bulk}}}{V}\int_0^{L_z}\phi(z)\,\mathrm{d}z\right] \tag{18}$$

Following the previous discussion, it can be seen that this quantity is expressed only through *invariant* parameters establishing correspondence between the mesoscopic and the atomistic representations of the studied system. The term in the brackets in eq 18 equals the total number of chains, per unit surface, present in an interfacial PE melt/graphite system of size L_z along the z direction. To facilitate the interpretation of the subsequent results, it is mentioned that low values of $n(z)$ denote a "starved" plane which is intersected only by a few polymer molecules, being indicative of a chain tendency to become parallel with the adsorbing substrate (i.e., assume "flat" conformations). On the other hand, high values of $n(z)$ indicate that many chains intersect the considered plane, a situation favored when the polymer molecules assume an elongated shape along the z-axis of the system.[55]

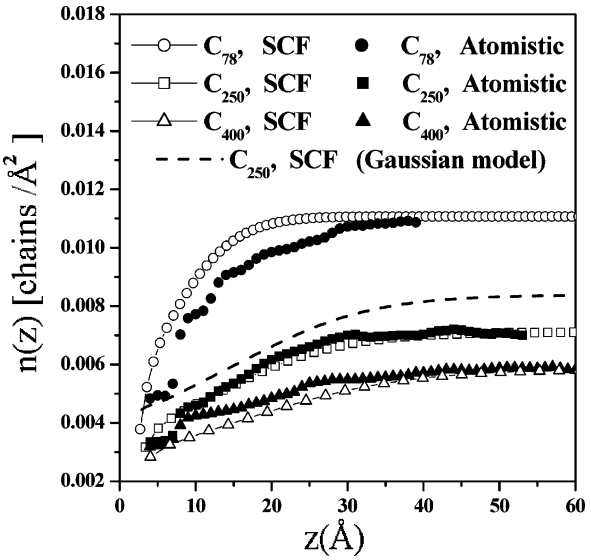

Figure 4. Chain shape profiles as derived by the SCF theory after the implementation of the wormlike chain connectivity model for the C_{78} (open circles), C_{250} (open squares), and C_{400} (open triangles) melts. The solid symbols display the corresponding atomistic simulation results, while the dashed line shows the predictions of the Gaussian model for the case of the C_{250} system.

The behavior of $n(z)$ as a function of distance from the adsorbing substrate as obtained from SCF calculations with the wormlike chain model and from atomistic simulations for the C_{78}, C_{250}, and C_{400} melts is shown in Figure 4. Taking into account the above discussion, the low values of the $n(z)$ parameter observed in the graphs of Figure 4 in the vicinity of the substrate are indicative of the prevalence of flattened chain conformations. With increasing distance from the adsorbing substrate, the conformations of the polymer chains become less flat and the bulk behavior is recovered approximately at distances equal to $1.5\sqrt{R_g^2}$, with R_g^2 being the mean-squared radius of gyration of the polymer. In particular, $n(z)$ assumes a constant value characteristic of the bulk polymer. This bulk value decreases with increasing chain length N as $1/\sqrt{N}$. This power law dependence is typical of polymer chains in a bulk melt in the long chain limit.

Figure 4 shows that, in the case of the C_{78} system, the SCF theory and the atomistic simulation exhibit a perceptible difference in the global conformational properties of the polymer chains, the molecules of the atomistic system assuming flatter conformations. On

the contrary, for the larger molecular weight systems the agreement between the two approaches improves significantly, so that the curves follow each other closely. This qualitative difference between low and higher molecular weights, which will be reinforced by the results presented subsequently, shows that the simplifications invoked in the formulation of the coarse-grained model are more crucial in the case of short molecules: The finite set of their conformations is too sensitive to the details of the force field to be fully described by the wormlike chain model. In comparison to the semiflexible model, the Gaussian model fails in a broader region of molecular weights. An example of the predictions of the Gaussian model for a C_{250} system is also presented in Figure 4. It can be observed that Gaussian molecules are less flat, so that the $n(z)$ profile remains always "higher" than both the simulation and the wormlike chain calculation results. Interestingly, the Gaussian model fails to reproduce even the bulk limit of $n(z)$ for the relatively low molecular lengths reported here. In particular, it predicts that more chains per unit surface should be crossing a plane placed in the bulk than is actually observed in the atomistic simulations and in the calculations with the wormlike chains. This discrepancy concerning the bulk behavior diminishes with increasing molecular length: for example, in the case of a C_{1000} melt system the difference between wormlike and Gaussian SCF limiting values of $n(z)$ in the bulk falls to 8%, compared to a 16% difference in the C_{250} melt.

Structure of Adsorbed Polymer Layer. One of the issues commonly addressed in a theoretical study of polymer adsorption is the characterization of conformations of adsorbed molecules in terms of tails, loops, and trains. More specifically, a molecule is considered as adsorbed when it has at least one adsorbed segment. In the current SCF calculations, a segment is defined as adsorbed when found within the attractive well of the polymer/solid interaction, while in the atomistic simulations any C−C bond with its middle at a distance less than 6 Å from the adsorbing graphite plane (that is in the first adsorption peak) is considered as adsorbed. In this way, practically, both coarse-grained and atomistic representations employ the same characteristic length for identifying adsorbed segments (see also Figures 1 and 2). After clarifying the concept of "adsorbed" segments, the definition of trains, tails, and loops follows straightforwardly along the lines presented in many previous publications (in refs 56 and 57, for instance).

The evaluation of the total volume fraction profile, $\phi_{ads}(z)$, of the segments belonging to adsorbed molecules as well as of the separate contributions of tails and loops can be carried out after decomposing[42] the wormlike or the Gaussian chain propagator, $q(z, s, \cos\theta)$ or $q(z, s)$, in two parts, q^{ads} and q^{free}, describing the adsorbed and free states, respectively, of the polymer molecule. The q^{free} propagator can be calculated from eq 9 (in practice, from the equivalent set of eqs 15a,b) or from eq 10, depending on the chain connectivity model, with proper initial and boundary conditions: $q^{free}(z, 0, \cos\theta) = 1$, where $w < z < L_z$ and $q^{free}(w, s, \cos\theta) = 0$, $q^{free}(L_z, s, \cos\theta) = 1$. (The reader is reminded that w is the width of the attractive well.) In this way the q^{ads} part is easily obtained after subtracting the q^{free} propagator from the total one: $q^{ads} = q - q^{free}$. The volume fraction profile of the free, $\phi_{free}(z)$, and the adsorbed polymer, $\phi_{ads}(z)$, as well as the contributions of tails, $\phi_{tails}(z)$, and loops, $\phi_{loops}(z)$, are obtained[42] as

$$\phi_{free}(z) = \frac{1}{2}\int_{-1}^{1}\int_{0}^{1} q^{free}(z, s, \cos\theta)\, q^{free}(z, 1-s, -\cos\theta)\, ds\, d\cos\theta \quad (19a)$$

$$\phi_{ads}(z) = \frac{1}{2}\int_{-1}^{1}\int_{0}^{1} q^{ads}(z, s, \cos\theta)\, q^{ads}(z, 1-s, -\cos\theta)\, ds\, d\cos\theta \quad (19b)$$

$$\phi_{loop}(z) = \frac{1}{2}\int_{-1}^{1}\int_{0}^{1} q^{ads}(z, s, \cos\theta)\, q^{ads}(z, 1-s, -\cos\theta)\, ds\, d\cos\theta, \quad z > w \quad (19c)$$

$$\phi_{tails}(z) = \int_{-1}^{1}\int_{0}^{1} q^{free}(z, s, \cos\theta)\, q^{ads}(z, 1-s, -\cos\theta)\, ds\, d\cos\theta, \quad z > w \quad (19d)$$

The results of these calculations regarding the volume fractions $\phi_{free}(z)$ and $\phi_{ads}(z)$ for the C_{78}, C_{250}, and C_{400} systems are shown in Figure 5 with the corresponding atomistic simulation data. In the same figures, the predictions derived with the Gaussian connectivity model are also reproduced. Obviously, for the smallest molecular length a significant part of the atomistic $\phi_{ads}(z)$ profile is dominated by the characteristic oscillations originating from monomer packing close to the substrate. It can be appreciated that the results concerning the global conformational properties of the adsorbed molecules will be subject to the small length scale details of the molecular model, so the discrepancy between the predictions of the wormlike chain model and the atomistic simulation is quite natural. As one proceeds to systems of longer chains, the agreement between atomistic simulation and wormlike chain SCF analysis improves considerably, and in the case of the C_{400} melt the two sets of results are very close to each other. Regarding the Gaussian chain connectivity model, the general conclusion from the graphs of Figure 5 is that the results obtained for low molecular weights exhibit a larger divergence from the atomistic simulation data than those of the wormlike chain model. Taking into account the comparison for the longest C_{400} melt, however, it can be appreciated that the predictive power of the Gaussian model also improves with increasing chain length.

Figure 6 shows the $\phi_{loop}(z)$ and $\phi_{tails}(z)$ contributions to the total $\phi_{ads}(z)$ profile as obtained from atomistic simulations and SCF calculations with both chain connectivity models for the C_{78}, C_{250}, and C_{400} melts. It is observed that, according to the atomistic simulations, for small chain lengths the total adsorption profile should be dominated by segments belonging to the free tails of adsorbed chains, even close to the substrate. Only in the case of the C_{400} system is $\phi_{loop}(z)$ nearly equal to $\phi_{tails}(z)$ near the first adsorption layer. For systems with longer chains, the loop contribution to $\phi_{ads}(z)$ is expected to prevail over the tail component in the vicinity of the substrate until a characteristic distance, usually denoted[42] as z^*, is reached. Considering the SCF calculations, the implementation of the wormlike chain model leads to a much better agreement with the simulation data in comparison with the Gaussian model. In particular for the longest melt, i.e., the C_{400}, the wormlike chains reproduce the atomistic $\phi_{loop}(z)$ and $\phi_{tail}(z)$ profiles very closely. On the contrary, the implementation of the Gaussian model is characterized

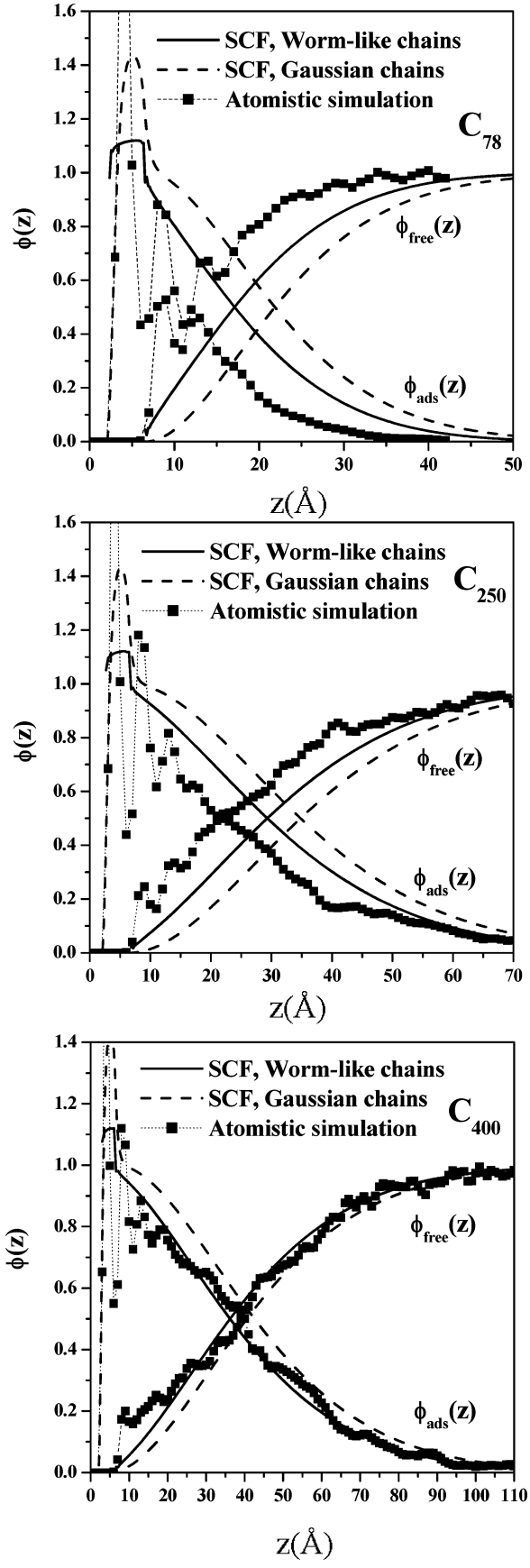

Figure 5. Volume fraction profiles of segments belonging to adsorbed, $\phi_{ads}(z)$, and free, $\phi_{free}(z)$, chains as derived by the SCF theory after the implementation of the wormlike (solid line) and the Gaussian (dashed line) chain connectivity models for the C_{78}, C_{250}, and C_{400} melts. The solid symbols display the corresponding atomistic simulation results.

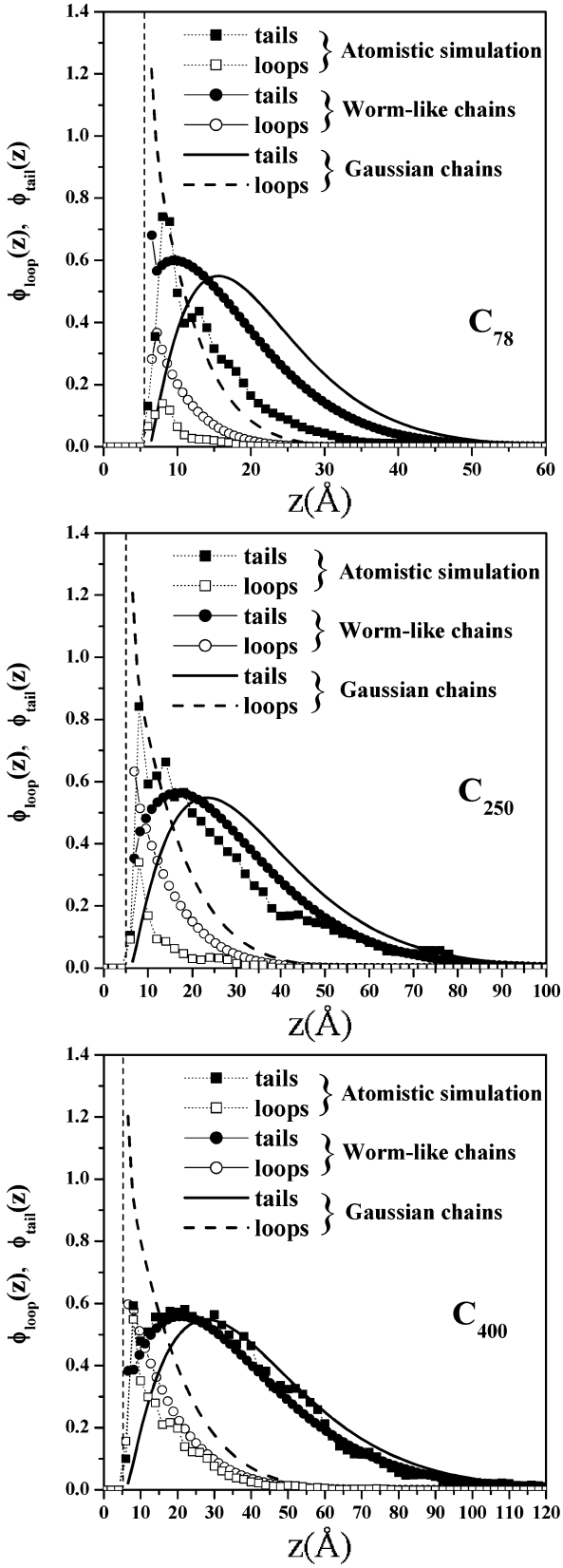

Figure 6. Volume fraction profiles of segments belonging to tails, $\phi_{tail}(z)$, and loops, $\phi_{loop}(z)$, as derived by the SCF theory after the implementation of the wormlike (solid circles and open circles) and the Gaussian (solid line and dashed line) chain connectivity models for the C_{78}, C_{250}, and C_{400} melts. The solid and open squares show the corresponding atomistic simulation results for the tails and loops, respectively. The vertical, thin dashed line marks the boundary of the region where the polymer is subjected to the effects of the attractive square well potential in the coarse-grained description.

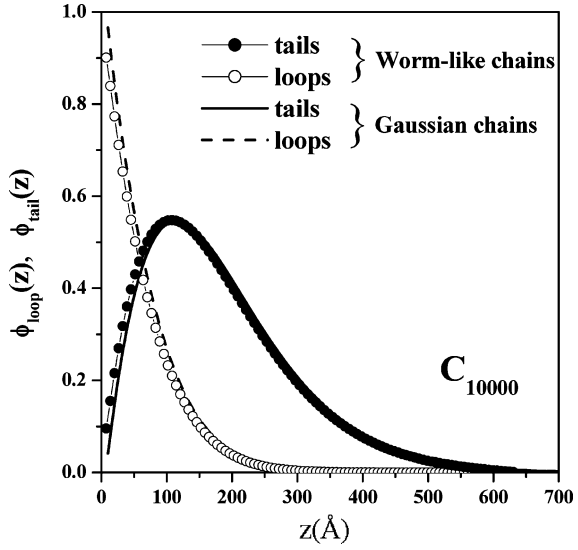

Figure 7. Volume fraction profiles of segments belonging to tails, $\phi_{tails}(z)$, and loops, $\phi_{loops}(z)$, as derived by the SCF theory after the implementation of the wormlike (solid circles and open circles) and the Gaussian (solid line and dashed line) chain connectivity models for the case of a C_{10000} melt.

by a noticeable overestimation of loop contribution close to the substrate, predicting a deep depletion of tails close to it. Even in the C_{400} system, although the Gaussian model grasps the functional form and the correct length scales of the $\phi_{tail}(z)$ profile in the outer region of the adsorbed layer, it rather fails in the inner part of it. This can be understood if one considers that for the formation of loops it is critical for the polymer molecule to "bend" in order to revisit the immediate vicinity of the surface. Since there is no bending penalty in the Gaussian model and the bonds are infinitely extensible, it is much easier for the Gaussian coarse-grained molecules to return to the substrate compared to the atomistic polymer chains. As a consequence, $\phi_{loop}(z)$ is considerably overestimated for the relatively short molecular lengths reported in Figure 6. As one proceeds to adsorbed PE melts with molecular lengths higher than C_{1000}, differences between the predictions of the Gaussian and the wormlike chains concerning the structure of the layer formed by the adsorbed polymer chains become less significant. To illustrate this, the results of SCF calculations for the $\phi_{loop}(z)$ and $\phi_{tail}(z)$ profiles derived by both models are presented in Figure 7 for the case of an adsorbed C_{10000} melt. It can be seen that, in this limit, the predictions of the two models are nearly identical although, close to the surface, differences are still perceptible.

The $\phi_{ads}(z)$, $\phi_{loop}(z)$, and $\phi_{tail}(z)$ profiles of Figures 5 and 6 can be utilized to derive the average fraction of segments ν_{tails}, ν_{loops}, and ν_{trains} of an adsorbed chain contained in tails, loops, and trains, respectively. The profiles are integrated over the z coordinate to obtain the volumes per unit surface of (a) adsorbed polymer, Γ, (b) adsorbed polymer contained in loops, Γ_{loops}, and (c) adsorbed polymer contained in tails, Γ_{tails}. Then, the fractions ν_{tails}, ν_{loops}, and ν_{trains} can be derived[58] as $\nu_{tails} = \Gamma_{tails}/\Gamma$, $\nu_{loops} = \Gamma_{loops}/\Gamma$, and $\nu_{trains} = (\Gamma - \Gamma_{tails} - \Gamma_{loops})/\Gamma$. The results for various chain lengths, N, as determined from both the wormlike and the Gaussian chain connectivity models, are presented in Figure 8 as log/linear plots. In the same graph, the atomistic simulation results for the C_{78}, C_{250}, and C_{400} melts are also shown. It can be appreciated that, for all the three fractions, the SCF results obtained through the wormlike chain model are much closer to the atomistic simulation results than the predictions from the Gaussian chain connectivity representation. In the case of wormlike chains the ν_{tails} fraction, for large chain lengths, tends asymptotically to a fixed value estimated to be around 0.67.

Nearly the same limiting value for ν_{tails} was obtained by Scheutjens and Fleer,[56] who incorporated the discussion of adsorbed melts in their lattice SCF study of polymer adsorption from solution, as a limiting case of zero solvent concentration. In this limit they established a direct correspondence between the findings of the lattice SCF theory concerning the conformations of adsorbed polymer chains with the predictions of the theory of Roe[59] referring to isolated adsorbed molecules, in the special case when the energy of monomer−solid

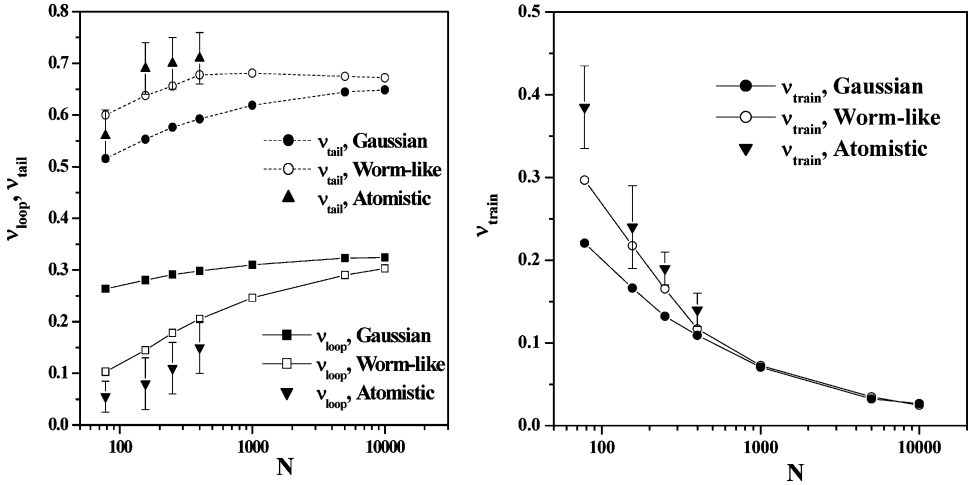

Figure 8. Average fraction of segments belonging to adsorbed chains found in tails, ν_{tail}, loops, ν_{loop} (left), and trains, ν_{train} (right), reported as a function of chain length. On the left graph, open circles and squares display the SCF predictions derived from the wormlike chain model for tails and loops, respectively, while filled circles and squares display the SCF predictions from the Gaussian connectivity model. Also on the right graph, open and filled circles display the predictions of the wormlike and Gaussian chain models, respectively, for the fraction of trains. Solid triangles, on both graphs, show the atomistic simulation results.

substrate interaction equals the critical adsorption energy. According to the conclusions of Roe,[59] ≈70% of segments of the adsorbed chain should be distributed between two long tails. The rest, located in the middle of the chain, should form loops and trains. The average length of loops should scale as $N^{1/2}$, while the trains should be of some small finite length being independent of N.

In the framework of the conformational properties of the adsorbed molecules presented above, it is expected that for large N, apart from ν_{tails}, ν_{loops} will also asymptotically reach some fixed value. This can be appreciated after considering that in an adsorbed melt the polymer chains are expected, effectively, to follow reflected random walk statistics[60] (despite the fact that the *microscopic* boundary condition for the chain propagator is the absorbing one), so the number of a chain's contact points with the substrate will scale as $N^{1/2}$. Since the loops are located between the contact points, their total number per chain should also scale as $N^{1/2}$. Considering the dependence of loop average length on N given by Roe, one concludes that the total number of segments located in loops should depend linearly on N. After dividing by total chain length, the asymptotic scaling dependence of ν_{loops} on N is obtained as $\nu_{\text{loops}} \sim N^0$, i.e., constant.

In the case of the wormlike chains it can be observed from Figure 8 that, while ν_{tails} reaches "saturation" quite fast (for melts longer than the C_{1000} it is practically constant), ν_{loops} still changes considerably over the studied range of molecular lengths. The atomistic simulation results seem to confirm this trend, although it was, of course, impossible to reach the molecular lengths considered in the SCF calculations. The Gaussian model, contrary to the semiflexible chains, considerably overestimates the fraction of ν_{loops} for the low molecular weight melts, while at the same time it underestimates the tail contribution. In addition, ν_{loops} in the Gaussian SCF model reaches the "saturation plateau" too fast: it is practically constant for melts longer than C_{1000}. As a general conclusion, it can be said that the discrepancies between the predictions of the Gaussian model concerning the conformational properties of the adsorbed chains when compared to the wormlike chain model results and the atomistic simulation data are more significant for loops than for tails. This is also supported by the graphs of Figure 6 showing the $\phi_{\text{loop}}(z)$ and $\phi_{\text{tail}}(z)$ profiles. Also, the agreement between the two coarse-grained models is better concerning the ν_{train} fraction; it can be observed that, beyond the C_{250} melt, their predictions for this fraction are close to each other and to the atomistic simulation results.

The data on the tail fraction, ν_{tails}, can be further utilized for the calculation of the average tail length, after the number of tails per chain is calculated. To evaluate the number of tails per chain, it is convenient to calculate an auxiliary propagator, $\tilde{q}(z, s, \cos\theta)$, which is defined from the solution of eq 9 (in practice, of its equivalent form eq 15a,b) after substituting the solution of the SCF scheme, $W(z)$, with initial conditions $q(z, 0, \cos\theta) = 0$, $0 < z \le w$, and $q(z, 0, \cos\theta) = 1$, $w < z < L_z$, while the boundary conditions remain the same as for the $q(z, s, \cos\theta)$ propagator. This auxiliary propagator will be proportional to the number of chain conformations that have one nonadsorbed (i.e., "free") end, while there is no restriction on the location of the second one. It is then possible to calculate the probabilities p_0, p_1, and p_2 that the adsorbed chain will have no tails, only one tail, and two tails, respectively. These are found as

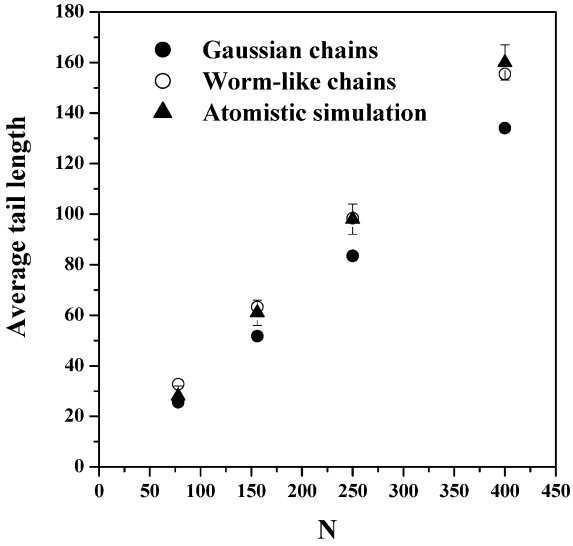

Figure 9. Average tail length reported as a function of chain length. The open and the solid circles display the SCF theory predictions derived from the wormlike and the Gaussian chain connectivity models, respectively. The solid triangles show the corresponding atomistic simulation results.

$$p_1 = 2\,\frac{\int_0^w \int_{-1}^1 \tilde{q}(z, 1, \cos\theta)\,\mathrm{d}\cos\theta\,\mathrm{d}z}{\int_0^{L_z} \int_{-1}^1 q^{\text{ads}}(z, 1, \cos\theta)\mathrm{d}\cos\theta\,\mathrm{d}z}$$

$$p_2 = \frac{\int_{-1}^1 \{\int_w^{L_z} [\tilde{q}(z, 1, \cos\theta) - q^{\text{free}}(z, 1, \cos\theta)]\,\mathrm{d}z\}\,\mathrm{d}\cos\theta}{\int_0^{L_z} \int_{-1}^1 q^{\text{ads}}(z, 1, \cos\theta)\,\mathrm{d}\cos\theta\,\mathrm{d}z}$$

$$p_0 = 1 - p_1 - p_2 \tag{20}$$

After this, the average number of tails per chain, n_{tail}, is trivially evaluated as $n_{\text{tail}} = p_1 + 2p_2$ so that the chain fraction per tail is given as $\nu_{\text{tails}}/n_{\text{tail}}$. This is an *invariant* quantity, and the average tail length of an atomistic chain is calculated as $N\nu_{\text{tails}}/n_{\text{tail}}$.

The predictions concerning the average tail length obtained from the above calculation for the case of the wormlike and the Gaussian chain connectivity models are shown in Figure 9. On the same figure, the atomistic simulation results for the C_{78}, C_{156}, C_{250}, and C_{400} melts are also reproduced. It can again be observed that the predictions for the average tail length derived through the wormlike chain model are closer to the atomistic simulation results. Nevertheless, the initial divergence observed between the predictions of the two coarse-grained models diminishes for melts consisting of longer chains (not shown on the graph). For example, in the case of the C_{10000} melt the predictions of the Gaussian and the wormlike chain models for the average tail lengths are 3385 and 3444, respectively.

7. Summary and Conclusions

In this work, the problem of determining the equilibrium properties of a polymer melt of specific chemical constitution, adsorbed on a certain solid substrate through a continuum SCF approach, was considered.

Monomer−monomer interactions were introduced by considering the polymer melt as compressible with density variations being driven by a harmonic penalizing potential suggested by Helfand and co-workers.[23−25] This approach is quite simplified and does not account for local monomer packing effects, which can be particularly important to some aspects of structure in the close vicinity of the adsorbing substrate, such as the spatial variations of the local density. In this direction a possible future improvement could come from "borrowing" the interaction potential from a density functional theory and subsequently incorporating it into the SCF formalism.[4,31−33] The interaction potential between the polymer and the substrate could have been described by preserving the original functional form of the atomistic polymer/substrate interaction, after tuning the parameters so as to reproduce the total energy of adsorption per unit surface of the atomistic polymer/solid interfacial system. Instead, in the current work the simple functional form of square well was employed. The parameters of the latter (width and depth) were tuned to reproduce the total energy of adsorption and the characteristic length scale of the density variations of the atomistic system. This proved adequate for our case; however, care should be taken when addressing systems with long-range polymer/substrate interactions, where the square-well approximation may not be applicable.

The chain connectivity was represented through the wormlike chain model, which has the advantage of reproducing on the coarse grained level both the mean-squared end-to-end distance and the contour length of the atomistic polymer molecule. Although this model has been used in several studies of interfacial polymeric systems,[9,10,37] to the best of our knowledge, this is the first time it is implemented in the framework of a SCF treatment of a polymer adsorption problem. The Gaussian chain connectivity model reproducing the mean-squared end-to-end distance in the bulk was also considered in the SCF analysis, and results from it were compared to the predictions of the wormlike chain model.

After the specification of the coarse-grained representation, the SCF formalism was cast in terms of several parameters, the *invariants* of the mesoscopic representation, establishing correspondence between the atomistic polymeric system and its coarse-grained counterpart. The formulation is general. It has been implemented for the specific case of linear polyethylene melts adsorbed on graphite, since the availability of recent atomistic simulation data[13,14] offered a means of evaluating the SCF theoretical approach. The solution of the SCF formalism was performed through an iterative scheme, requiring at each step the determination of the conformations of the wormlike chain in the mean field. These conformations were described through a differential equation formulated[8] by Saito et al., which constitutes the analogue of the Edwards equation for wormlike chains. The numerical solution of this formulation was achieved through a combined spectral and real-space approach.[37] Instabilities close to the adsorbing boundary required the development of a new Lax−Wendroff-type numerical solution method.

During the SCF study various monodisperse melts were considered, ranging from C_{78} to C_{10000}, with particular emphasis on molecular weights allowing a direct comparison with the atomistic simulation data. After solving the SCF equation set, it was possible to characterize the chain conformations through a variety of descriptors. Both the wormlike and the Gaussian chain SCF approaches as well as the atomistic simulations showed that the polymeric chains become significantly "flattened" near the boundary. Generally, perturbations in their conformational properties due to the surface persist over a characteristic length which is roughly 1.5 times the mean gyration radius of the unperturbed polymer molecule in the bulk. It was observed that, even for the relatively short chain melts addressed in the atomistic simulations (up to C_{400}), SCF predictions using the wormlike chain model concerning the degree of flattening of the polymeric molecules are much closer to simulation results that those from the Gaussian model. In particular, starting from the C_{250} melt, the wormlike SCF model predictions capture the simulation results quite well, contrary to the Gaussian chain model, which underestimates the degree of chain flattening even for the longest C_{400} system. It is clarified, however, that in the case of the shortest chain melts (i.e., C_{78}) the results are too much dominated by the atomistic details of the molecular model to be approximated reliably by any of the two coarse-grained representations that were implemented.

The conformations of adsorbed molecules were further characterized by considering the properties of tails, loops, and trains, as derived by SCF analysis from the two coarse-grained models and from the atomistic simulations. It was observed that the discrepancies between the predictions of the Gaussian chain model and the atomistic simulation data remain significant in the entire range of simulated molecular lengths (i.e., up to C_{400}). The failure of the Gaussian model in this region is particularly evident in the case of loops, whose contribution to the adsorbed polymer layer it considerably overestimates. On the other hand, as regards the properties of the outer region of the adsorbed polymer layer formed by the dangling tails of the adsorbed molecules, SCF predictions from the Gaussian model improve fast with increasing molecular weight. At the same time, SCF predictions from the wormlike chain model are much closer to the atomistic simulation results; in the case of the longest C_{400} system, agreement between wormlike SCF and atomistic simulation predictions is quantitatively very good concerning both tails and loops. The superior performance of the semiflexible chain model when compared to the Gaussian one, in all cases considered, can be explained after taking into account that the former model is characterized by an additional length scale on the level of chain persistence length. The incorporation of this intermediate length scale brings the wormlike chain closer to the atomistic molecule, improving its predictive capabilities concerning the structure of loops. With increasing molecular length, the effect of the local chain structure (i.e., of small length scale properties) on global chain conformational behavior decreases. Thus, for melts consisting of long polymer chains (C_{10000}, for instance), the difference between the chain level structures predicted by the two coarse-grained models becomes insignificant.

Acknowledgment. We are grateful to the General Secretariat of Research and Technology of Greece for financial support through a PENED program, No. 01EΔ529.

Appendix. Numerical Solution of the Wormlike Chain Propagator Equation

As was mentioned in the main text, the principal numerical difficulty encountered in the current work was the solution of eqs 15a,b obtained after expressing the propagator $q(z, s, \cos\theta)$ in terms of Legendre polynomials (eq 14).

After the truncation of the Legendre polynomial series, the set of differential equations (eqs 15a,b) becomes finite and can be solved through an explicit Lax−Wendroff-type technique.[53] The suggested approach following the standard Lax−Wendroff method for hyperbolic equations employs a discretization of space and time domains through some regular grid. Next, it relies on the observation[53] that, when the partial derivatives with respect to s and z in eq 15a are approximated through first-order forward and second-order central finite difference schemes, respectively, the resulting equation will not correspond to the original eq 15a but to the equation

$$\frac{2\eta}{N}\frac{\partial \tilde{q}_l}{\partial s} = -\left[\frac{l}{2l-1}\frac{\partial \tilde{q}_{l-1}}{\partial z} + \frac{l+1}{2l+3}\frac{\partial \tilde{q}_{l+1}}{\partial z}\right] - (l+1)l\tilde{q}_l - \frac{2\eta}{N}W(z)\tilde{q}_l - \frac{2\eta\Delta s}{N\ 2}\frac{\partial^2 \tilde{q}_l}{\partial s^2}, \quad l = 0, ..., l_{\text{trunc}} \quad \text{(A1)}$$

where l_{trunc} denotes the moment after which the Legendre polynomials series is truncated (i.e., in our case $l_{\text{trunc}} = 7$). Thus, in the finite difference analogue of eqs 15a,b, the term $(2\eta/N)(\Delta s/2)(\partial^2\tilde{q}_l/\partial s^2)$ should be *added* to the right-hand side of the equation to cancel out the $-(2\eta/N)(\Delta s/2)(\partial^2\tilde{q}_l/\partial s^2)$ component. For its representation, the second-order derivative $(\partial^2\tilde{q}_l/\partial s^2)$ is expressed from eq 15a as

$$\frac{2\eta}{N}D_{ss}\tilde{q}_l = -\left[\frac{l}{2l-1}D_{sz}\tilde{q}_{l-1} + \frac{l+1}{2l+3}D_{sz}\tilde{q}_{l+1}\right] - (l+1)lD_s\tilde{q}_l - \frac{2\eta}{N}W(z)D_s\tilde{q}_l, \quad l = 0, ..., l_{\text{trunc}} \quad \text{(A2)}$$

where, for convenience, the operators D_{ab} have been introduced to denote the second-order partial derivatives of the function $\tilde{q}_l$ with respect to the variables a and b. The functions $D_{sz}\tilde{q}_{l-1}$ and $D_{sz}\tilde{q}_{l+1}$ in eq A.2 can be substituted with their equivalent form obtained after differentiating the right-hand side of eq 15a with respect to z as

$$\frac{2\eta}{N}D_{sz}\tilde{q}_{l-1} = -\left[\frac{l-1}{2l-3}D_{zz}\tilde{q}_{l-2} + \frac{l}{2l+1}D_{zz}\tilde{q}_l\right] - (l-1)lD_z\tilde{q}_{l-1} - \frac{2\eta}{N}D_z[W(z)\tilde{q}_{l-1}]$$

$$\frac{2\eta}{N}D_{sz}\tilde{q}_{l+1} = -\left[\frac{l+1}{2l+1}D_{zz}\tilde{q}_l + \frac{l+2}{2l+5}D_{zz}\tilde{q}_{l+2}\right] - (l+1)(l+2)D_z\tilde{q}_{l+1} - \frac{2\eta}{N}D_z[W(z)\tilde{q}_{l+1}] \quad \text{(A3)}$$

where it is clarified that $\tilde{q}_l = 0$ for $l \notin [0, l_{\text{trunc}}]$. After the above manipulations, the finite-difference scheme is formulated by adding to eq 15a the term $(2\eta/N)(\Delta s/2)(\partial^2\tilde{q}_l/\partial s^2)$ being expressed only through the D_s, D_z, and the D_{zz} differential operators. Next, in this "transformed" eq 15a an approximation to the D_s, D_z, and D_{zz} derivatives is performed through first-order forward, second-order central, and second-order central second differences, respectively, and an algebraic expression for $\tilde{q}_l(s + \Delta s, z)$ is obtained. The repeated application of this expression delivers the desired time-marching solution $\tilde{q}_l(s,z)$, $l = 0, ..., l_{\text{trunc}}$, of the propagator equation (eqs 15a,b).

References and Notes

(1) Aoyagi, T.; Honda, T.; Doi, M. *J. Chem. Phys.* **2002**, *117*, 8153.
(2) Terzis, A. F.; Theodorou, D. N.; Stroeks, A. *Macromolecules* **2000**, *33*, 1385; **2000**, *33*, 1397; **2002**, *35*, 508.
(3) Theodorou, D. N. *Macromolecules* **1989**, *22*, 4578; **1989**, *22*, 4589.
(4) Schmid, F. *J. Phys.: Condens. Matter* **1998**, *10*, 8105.
(5) Bonet-Avalos, J.; Mackie, A. D.; Diez-Orrite, S. *Macromolecules* **2004**, *37*, 1124, 1143.
(6) Carigano, M. A.; Szleifer, I. *J. Chem. Phys.* **1993**, *98*, 5006.
(7) Carigano, M. A.; Szleifer, I. *Colloids Surf. B* **2000**, *18*, 169.
(8) Saito, N.; Takahashi, K.; Yunoki, Y. *J. Phys. Soc. Jpn.* **1966**, *22*, 219.
(9) Morse, D. C.; Fredrickson, G. H. *Phys. Rev. Lett.* **1994**, *73*, 3235.
(10) Matsen, M. W. *J. Chem. Phys.* **1996**, *104*, 7758.
(11) Daoulas, K. Ch.; Terzis, A. F.; Mavrantzas, V. G. *J. Chem. Phys.* **2002**, *116*, 11028.
(12) Frischknecht, A. L.; Curro, J. G. *J. Chem. Phys.* **2004**, *121*, 2788.
(13) Daoulas, K. Ch.; Harmandaris, V. A.; Mavrantzas, V. G. *Macromolecules*, **2005**, *38*, 5780.
(14) Harmandaris, V. A.; Daoulas, K. Ch.; Mavrantzas, V. G. *Macromolecules*, **2005**, *38*, 5796.
(15) Martin, M. G.; Siepmann, J. I. *J. Phys. Chem. B* **1998**, *102*, 2569.
(16) van der Ploeg, P.; Berendsen, H. J. *J. Chem. Phys.* **1982**, *76*, 3271.
(17) Toxvaerd, S. *J. Chem. Phys.* **1997**, *107*, 5197.
(18) Steele, W. A. *Surf. Sci.* **1973**, *36*, 317.
(19) Pant, P. V. K.; Theodorou, D. N. *Macromolecules* **1995**, *28*, 7224.
(20) Mavrantzas, V. G.; Boone, T. D.; Zervopoulou, E.; Theodorou, D. N. *Macromolecules* **1999**, *32*, 5072.
(21) Karayiannis, N. Ch.; Mavrantzas, V. G.; Theodorou, D. N. *Phys. Rev. Lett.* **2002**, *88*, 105503.
(22) Wu, D. T.; Fredrickson, G. H.; Carton, J. P.; Ajdari, A.; Leibler, L. J. *Polym. Sci., Part B: Polym. Phys.* **1995**, *33*, 2373.
(23) Helfand, E. *Macromolecules* **1975**, *8*, 552.
(24) Helfand, E.; Sapse, A. *J. Chem. Phys.* **1975**, *62*, 1327.
(25) Helfand, E.; Wasserman, Z. R. *Macromolecules* **1978**, *11*, 960.
(26) Yethiraj, A.; Woodward, E. *J. Chem. Phys.* **1995**, *102*, 5499.
(27) Frischknecht, A. L.; Weinhold, J. D.; Salinger, A. G.; Curro, J. G.; Douglas Frink, L. J.; McCoy J. D. *J. Chem. Phys.* **2002**, *117*, 10385, 10398.
(28) Yu, Y. X.; Wu, J. Z. *J. Chem. Phys.* **2002**, *117*, 2368.
(29) Patra, C. N.; Yethiraj, A. *J. Chem. Phys.* **2003**, *118*, 4702.
(30) Brik, P.; Bucior, K.; Sokolovski, S.; Zukocinski, G. *J. Phys. Chem. B* **2005**, *109*, 2977.
(31) Müller, M.; MacDowell, L. G.; Yethiraj, A. *J. Chem. Phys.* **2003**, *118*, 2929.
(32) Schmid, F. *J. Chem. Phys.* **1996**, *104*, 9191.
(33) Müller, M.; MacDowell, L. G. *Macromolecules* **2000**, *33*, 3902.
(34) Fredrickson, G. H.; Ganesan, V.; Drolet, F. *Macromolecules* **2002**, *35*, 16.
(35) Müller, M.; Schmid, F. *Adv. Polym. Sci.*, in press.
(36) Chen, Z. Yu. *Macromolecules* **1993**, *26*, 3419.
(37) Müller, M.; Schmid, F. *Macromolecules* **2002**, *35*, 16.
(38) Kratky, O.; Porod, G. *Recl. Trav. Chim.* **1949**, *68*, 1106.
(39) Grosberg, A. Yu.; Khokhlov, A. R. *Statistical Physics of Macromolecules*; American Institute of Physics: New York, 1994.
(40) Helfand, E. *J. Chem. Phys.* **1975**, *62*, 999.
(41) Hong, K. M.; Noolandi, J. *Macromolecules* **1981**, *14*, 727.
(42) Semenov, A. N.; Bonet-Avalos, J.; Johner, A.; Joanny, J. F. *Macromolecules* **1996**, *29*, 2179.
(43) Gorbunov, A. A.; Skvortsov, A. M.; van Male, J.; Fleer, G. J. *J. Chem. Phys.* **2001**, *114*, 5366.
(44) van der Gucht, J.; Besseling, N. A. M.; Fleer, G. J. *Macromolecules* **2004**, *37*, 3026.
(45) de Gennes, P. G. *Rep. Prog. Phys.* **1969**, *32*, 187.
(46) Daoulas, K. Ch.; Theodorou, D. N.; Roos, A.; Creton, C. *Macromolecules* **2004**, *37*, 5093.
(47) Dee, G. T.; Ougizawa, T.; Walsh, D. J. *Polymer* **1992**, *33*, 3462.

(48) Karayiannis, N. Ch.; Giannousaki, A. E.; Mavrantzas, V. G.; Theodorou, D. N. *J. Chem. Phys.* **2002**, *117*, 5465.
(49) Drolet, F.; Fredrickson, G. H. *Macromolecules* **2001**, *34*, 5317.
(50) Drolet, F.; Fredrickson, G. H. *Phys. Rev. Lett.* **1999**, *83*, 4317.
(51) Press, W. H.; Vellerling, W. T.; Teukolsky, S. A.; Flannery, B. P. *Numerical Recipes*; Cambridge University Press: New York, 1992.
(52) Düchs, D.; Sullivan, D. E. *J. Phys.: Condens. Matter* **2002**, *14*, 12189.
(53) Smith, G. D. *Numerical Solution of Partial Differential Equations: Finite Difference Methods*; Clarendon Press: Oxford, 1985.
(54) Rivillon, S.; Auroy, P.; Deloche, B. *Phys. Rev. Lett.* **1999**, *84*, 499.
(55) Theodorou, D. N. *Macromolecules* **1988**, *21*, 1411.
(56) Scheutjens, J. M. H. M.; Fleer, G. J. *J. Phys. Chem.* **1979**, *83*, 1619; **1980**, *84*, 178.
(57) Fleer, G. J.; Cohen Stuart, M. A.; Scheutjens, J. M. H. M.; Cosgrove, T.; Vincent, B. *Polymers at Interfaces*; Chapman and Hall: Cambridge, 1993.
(58) Fleer, G. J.; van Male, J.; Johner, A. *Macromolecules* **1999**, *32*, 825.
(59) Roe, R. J. *J. Chem. Phys.* **1965**, *43*, 1591.
(60) Bitsanis, I. A.; ten Brinke, G. *J. Chem. Phys.* **1993**, *99*, 178.

MA050218B